Theoretical study of the thermodynamic and kinetic properties of self-interstitials in aluminum and nickel

Susana Ramos de Debiaggi,[1] Maurice de Koning,[2] and Ana María Monti[3]
[1]*Departamento de Física, Universidad Nacional del Comahue, Buenos Aires 1400, 8300 Neuquén, Argentina*
[2]*Instituto de Física Gleb Wataghin, Universidade Estadual de Campinas, Unicamp, 13083-970, Campinas, São Paulo, Brazil*
[3]*Departamento de Materiales, Comisión Nacional de Energía Atómica, Avenida Gral. Paz 1499, Casilla Postal B1650KNA, San Martín, Pcia. de Buenos Aires, Argentina*
(Received 16 June 2005; revised manuscript received 12 January 2006; published 7 March 2006)

The formation thermodynamics and migration properties of self-interstitials in aluminum and nickel are investigated as a function of temperature using atomistic simulation techniques and embedded-atom-type interatomic potentials. Molecular dynamics and nonequilibrium free-energy techniques are employed to investigate anharmonic effects on the H_O ⟨100⟩ dumbbell formation properties. The equilibrium concentration of this defect is compared to those of vacancies and divacancies. The results are then analyzed in the framework of the interstitialcy model, according to which very high vibrational formation entropies should be expected for self-interstitials at high temperatures. The kinetics of self-interstitial migration is also investigated using different atomistic techniques, revealing the simultaneous activity of more than one distinct interstitial configuration as the temperature increases.

DOI: 10.1103/PhysRevB.73.104103 PACS number(s): 61.72.Ji, 65.40.Gr, 02.70.Ns

I. INTRODUCTION

Knowledge of the structural and thermodynamic properties of point defects is of fundamental importance to understand different microstructural processes in crystalline solids. It is well known that the concentration of thermally formed vacancies in metals by far exceeds that of self-interstitial atoms (SIA's). According to thermodynamics, the thermal equilibrium concentration of an intrinsic defect in a crystal at temperature T is given by $c=g\exp-(H^f-TS^f)/k_BT$, where H^f and S^f are the enthalpy and entropy of formation, respectively, g is a geometrical factor, and k_B is the Boltzmann constant. The formation enthalpy of vacancies is relatively small compared to that of SIA's, which are of the order of several eV. In this case, assuming formation entropy values of similar magnitude, about a few k_B, the SIA's equilibrium concentration is expected to be much lower than the experimental detection limits, rendering vacancies the overwhelmingly dominant point-defect type in thermal equilibrium.[1]

On the other hand, Granato[2] in the interstitialcy theory of simple condensed matter states predicts that the interstitial concentration just below the melting temperature in the crystalline state should only be an order of magnitude smaller than the vacancy concentration, contrary to the usual assumption. The corresponding explanation points to the SIA's formation entropy value, which, according to estimates by Gordon *et al.*,[3,4] could be as high as $(10–20)k_B$.

In fcc metals the most stable self-interstitial configuration is the H_O ⟨100⟩ dumbbell,[5] also called interstitialcy. Its tetragonal symmetry and strong coupling to its nearest neighbors give rise to a vibrational spectrum with high-frequency localized modes and low-frequency resonant modes.[6] The latter lead to an unusually large entropy per defect. In addition, a large diaelastic softening of the shear modulus with defect concentration is derived, which leads to a decrease of its formation energy.[2,7] According to Gordon *et al.*,[3] the predictions of the interstitialcy model have been verified for krypton using lattice parameter measurements leading to an interstitial concentration of 7×10^{-4} near the triple point, and a formation entropy of approximately $16k_B$. More recently for aluminum, using elastic constant measurements,[4] an interstitial concentration of $(1.7\pm0.6)\times10^{-4}$ was obtained just below the melting temperature, leading to the estimates $H^f=2.5\pm0.5$ eV and $S^f=22k_B$ for the formation enthalpy and entropy, respectively.

The explicit temperature dependence of the formation enthalpy (and entropy) of point defects has been considered in different ways in the last decades, ranging from the simple linear for the enthalpy[8] to a stronger nonlinear dependence.[9] Recent progress in simulation techniques has come to show the importance of anharmonic effects in the properties of point defects. In particular, using atomistic simulation techniques that fully account for such anharmonic effects, the formation thermodynamics of vacancies and divacancies in Cu,[10] Al,[11–15] and Ni,[14,15] represented by empirical many-body potentials, were investigated. For the case of Al and Ni, for instance, the vacancy formation enthalpies at the melting point were found to be about 10% and 20% larger compared to their room-temperature values. An even stronger temperature dependence was observed for the formation entropies, which at the melting point were found to be a factor 2–3 times larger than the corresponding low-temperature values.[14]

Nordlund and Averback[16] have recently studied the formation of point defects in Cu through a direct counting approach along with molecular dynamics (MD) simulations. In their simulations, they used the empirical many-body potential of Sabochick and Lam,[17] which reproduces a wide range of vacancy and interstitial experimental properties. They obtain a reasonable value of a few eV for the interstitial formation enthalpy and a formation entropy value of $(15\pm2)k_B$, in agreement with the estimation of Granato. As a result, for

temperatures close to the melting point, the interstitial concentration is found to be as high as one-tenth of the vacancy concentration. The authors find that this trend is also reproduced in Cu and Au represented by the Foiles *et al.* embedded-atom-model (EAM) potential.[18]

A direct consequence of the high interstitial concentration may be its contribution to the self-diffusion data at elevated temperatures. This point is particularly interesting in relation to the well-known upward curvature observed in the Arrhenius plots of some fcc metals like Al.[8] Although such a curvature has traditionally been attributed to the contribution of divacancies, this explanation has been recently put in doubt as *ab initio* calculations indicated the unstable character of the divacancy in Al.[11–13] Complementary to the divacancy contribution, the explicit anharmonic effects in the vacancy formation free energies at high temperatures[10–15] and the occurrence of multiple vacancy jumps, in addition to the single ones, have also been considered recently.[19] In this context, the results of Nordlund and Averback[16] point to the contribution of self-interstitials as another possible explanation of the observed curvature in the self-diffusion Arrhenius plot. In fact, they find that the contribution of interstitials at the melting point is approximately seven times larger than that of divacancies. However, Sandberg *et al.*[12] combine several theoretical methods to show that the self-diffusion in Al is solely due to vacancy migration for all temperatures up to the melting point. They found that the deviations from single Arrhenius dependence are due to anharmonicity and that the contribution from divacancies and interstitials is less than 1% of that from vacancies at the melting point.

The purpose of the present paper is to analyze thermal effects on the SIA properties by investigating the formation thermodynamics and migration properties of self-interstitials in Al and Ni as a function of temperature using atomistic simulation methods. As a first step, we use molecular statics (MS) to calculate the energies, volumes, and vibrational entropies associated with the formation of interstitials at 0 K. Then we apply standard thermodynamic integration (TI) and reversible-work (RW) methods to evaluate the interstitial formation free energies as a function of temperature. Moreover, we carry out MS and MD simulations to study the kinetics of interstitial migration. In particular, we compute the tracer self-diffusion coefficient through the Einstein relation. During the runs, all the atomic jump mechanisms are recorded and analyzed to determine their relative contributions at high temperatures.

To the best of our knowledge, no previous theoretical results on the thermal behavior of SIA's in Ni have been reported. The case of Al has already been studied by Sandberg *et al.*[12] and we reconsider their results by comparing them to the present RW predictions for the formation free energy.

The remainder of the paper has been organized as follows. Section II describes the details of the applied simulation methods. Section III presents the obtained results, followed by our conclusions in Sec. IV.

II. METHODOLOGY AND COMPUTATIONAL PROCEDURES

A. Molecular statics simulations

We utilize MS simulations, based on conjugate-gradient minimization, to compute the defect energies and relaxation volumes in crystallites subject to standard periodic boundary conditions under zero pressure. Perfect crystallites of $N=256$ atoms and defective crystallites of 257 atoms, the latter composed of 255 atoms initially located at their perfect lattice sites, and an H_O $\langle 100\rangle$ dumbbell interstitial, are used. Many-body potentials of the embedded-atom-model type are used to represent the interatomic interactions. We use the Ercolessi and Adams (EA) model for Al,[20] (note that the same potential is used in Refs. 11–14) and that due to Voter and Chen for Ni.[21] Both potentials predict a reasonable thermal behavior over a wide temperature range.

The vibrational formation entropies are calculated in the harmonic approximation (HA) by

$$S^f = k_B \sum_{i,\alpha} \ln\left(\frac{\omega^0_{i,\alpha}}{\omega_{i,\alpha}}\right), \tag{1}$$

where the eigenfrequencies $\omega^0_{i,\alpha}$ and $\omega_{i,\alpha}$ are the eigenvalues of the second-order force-constant matrix for the perfect lattice and the defect equilibrium configuration, respectively. In order to compare the same number of eigenfrequencies, the contribution of the perfect lattice is suitably renormalized. The force constants are evaluated according to Eq. (22) of Finnis and Sinclair[22] and the coupled oscillator[23] (or determinant) approximation. The atomic interactions with periodic images of the atoms that belong to the crystallite are also taken into account in the force-constant construction. Note that, although Eq. (1) is strictly valid at the classical limit of high temperatures, it is applied to zero-temperature defect relaxed configurations following standard practices.[10–15,19,23]

B. Thermodynamic integration

In the standard thermodynamic integration method,[24] the temperature variation of the formation entropy S^f is obtained by integrating the thermodynamic relationship

$$\left(\frac{\partial S^f}{\partial T}\right)_P = \frac{1}{T}\left(\frac{\partial H^f}{\partial T}\right)_P, \tag{2}$$

where P is the pressure and the other quantities have been previously defined. To carry out the integration process, H^f is computed at different temperatures, using independent equilibrium simulations for both computational cells, with and without the defect. For the self-interstitial case, the formation enthalpy is then computed as

$$H^f(P,T) = H_d(P,T) - \frac{N+1}{N} H_{crystal}(P,T), \tag{3}$$

where $H_{crystal}$ and H_d are the enthalpy of the perfect and defective lattices respectively.

Constant-NPT MD simulations based on the Berendsen thermostat[25] have been carried out in the temperature range between 0 and 900 K for Al, and between 0 and 1700 K for Ni. In the simulations the samples remain crystalline. Average values of the enthalpies were measured along 13 ns MD trajectories. To evaluate the associated formation entropy variation with temperature the formation enthalpies have been fitted to fourth-order polynomials allowing straightforward integration of Eq. (2).

In order to obtain the absolute formation entropy S^f at different temperatures and the corresponding free energy $G^f = H^f - TS^f$, the integration constant (S_0) must be known. It is common practice to adopt the HA for this purpose, assuming that the potential energy surface explored at low temperatures can be accurately represented by a second-order expansion in terms of the atomic displacements from the equilibrium positions.[14,15] However, due to the loss of inversion symmetry at a defect site, the expansion may involve non-negligible higher-order terms that are of the same order of magnitude as the second-order terms in the harmonic expansion.[26] In this case the HA may give incorrect results, even for low temperatures. To evaluate this situation, we adopt a direct free-energy difference method that gives "exact" results, subject to statistical errors only.

C. Reversible work calculations

In addition to the standard TI scheme, we utilize the reversible-work method to obtain a direct estimate of the formation free energy at any temperature. The method is based on the introduction of a coupled potential energy function V, which, aside from the particle positions, depends on an "artificial" coupling parameter[24] λ as follows:

$$V(\{\vec{r}_i\},\lambda) = \lambda V_{syst}(\{\vec{r}_i\}) + (1-\lambda)V_{ref}(\{\vec{r}_i\}). \tag{4}$$

Above, V_{syst} is the potential energy function of the system of interest and V_{ref} is the potential energy function of a reference system (for instance an Einstein crystal). In this manner, $V(\{\vec{r}_i\},\lambda)$ describes a continuous thermodynamic path coupling the system of interest to the reference. Analysis of the partition function of the system based on the potential in Eq. (4) then shows that the free-energy difference between the system of interest and the reference is given by

$$G_{syst} - G_{ref} = \int_0^1 d\lambda \left\langle \frac{\partial V}{\partial \lambda} \right\rangle_\lambda, \tag{5}$$

where the angular brackets indicate an ensemble average for the coupled system at a particular value of λ. Accordingly, the difference between the free energies of the system of interest and reference can be determined by computing the integral on the right-hand side of Eq. (5), which represents the reversible work required to transform the system of reference into the system of interest. Typically this is accomplished in the same fashion as in the TI method described above, running a number of independent equilibrium simulations for λ values between 0 and 1, computing the corresponding ensemble averages $\langle \partial V/\partial\lambda \rangle$, and then estimating the integral numerically. In contrast to the HA, this method is "exact" in that it explicitly includes all anharmonic effects.

An alternative approach to computing the integral in Eq. (5) is to replace the set of independent equilibrium simulations at different values of λ by a single simulation in which the coupling parameter λ is varied *dynamically* between 0 and 1.[14,15,27]

In this fashion, the free-energy difference is estimated according to

$$G_{syst} - G_{ref} \approx \int_0^{t_s} dt \frac{d\lambda}{dt}\frac{\partial V}{\partial \lambda}, \tag{6}$$

where t_s is the simulation time over which λ varies between 0 and 1 and the integration is done over *instantaneous* values of the phase function $\partial V/\partial\lambda$. Although the process is intrinsically irreversible and subject to dissipative entropy production, the results [i.e., the integral in Eq. (6)] usually converge quickly with increasing t_s, allowing an accurate calculation of the free-energy difference from a relatively short simulation.

In the particular case of point-defect formation free energies, we utilize a coupled potential energy function different from the one in Eq. (4) and compute the reversible work required to reversibly remove or insert an atom in an otherwise perfect crystal. For this purpose, for the EAM potentials used in this work, we introduce the functional form

$$V(\{\lambda_i\}) = \frac{1}{2}\sum_{i,j} \lambda_i\lambda_j\phi(r_{ij}) + \sum_i U\left(\sum_j \lambda_i\lambda_j\rho(r_{ij})\right), \tag{7}$$

with ϕ the pair potential, ρ the electron density, and U the embedding function. For instance, in order to continuously switch off one atom within this functional form we introduce a set of coupling parameters λ_i for each atom, which measure the strength of the interactions between an atom and its neighbors. If all $\lambda_i=1$, the system is fully interacting. But if we set $\lambda_i=1\ \forall\ i\neq k$, $\lambda_k=0$, atom k does not interact with the remainder of the system. In this manner, a vacancy on lattice site k (or an interstitial on interstitial site k) is created by slowly switching λ_k from 1 to 0 (or from 0 to 1) while keeping all others equal to unity. By measuring the reversible work using (5) or (6) (with $\partial V/\partial\lambda_k$) one can then compute the reversible work at constant volume or pressure at a fixed temperature. This value represents the work necessary to remove (add) one atom from (to) the system. However, the formation free energy is defined as the difference between the system with the defect, and a perfect crystal with the same numbers of atoms. One must therefore still subtract (for the vacancy) or add (for the interstitial case) the free energy of one atom in the perfect crystal. This free energy can be computed very effectively using the reversible-scaling technique.[27] More details about this method can be found in Refs. 14 and 15.

D. Defect migration

To study self-interstitial migration, MD simulations are performed to evaluate the temperature dependence of the tracer diffusion coefficient D^T and obtain information about the jump mechanism. The atomic migration contribution to D^T is calculated through the Einstein relation

$$D^* = \lim_{t\to\infty} \frac{\langle r^2(t)\rangle}{6t}, \tag{8}$$

where $\langle r^2(t)\rangle$ is the mean-square displacement of all the atoms at time t. The size of the computational cells employed for these calculations is similar to those used for the previously described methods.

As will be shown in the next section, the $H_O\langle 100\rangle$ dumbbell is found to be the most stable SIA configuration for both EAM used in this work. For each temperature we first equilibrate the defect system, as well as the perfect lattice reference system, within the zero-pressure isobaric-isothermal ensemble. Subsequently, we follow the system's evolution under these conditions for a time interval that is sufficiently long to obtain reasonable jump statistics. Typically, several hundreds of jumps were observed for each temperature in simulations of up to 3 ns, the lower simulated temperatures being 300 K for Al and 400 K for Ni. The jumps are identified by checking, at each time step, the occupation number of the Wigner-Seitz cells in the reference lattice. Every time the occupation number changes, a jump is produced. Correlated jump sequences that do not effectively contribute to diffusion such as oscillations, in which an atom leaves its lattice site but almost immediately returns to it, are filtered out.[19] In this way, the associated defect migration energy can be evaluated from both the Arrhenius plot of D^* as a function of temperature as well as from the jump frequency $\Gamma = k\nu \exp -(H^m - TS^m)/k_B T$, where ν is the attempt frequency, S^m and H^m are the defect migration entropy and enthalpy, respectively, and k is the jump multiplicity.

In addition to the MD simulations we also use a standard MS procedure, the quasistatic approximation, to determine the defect migration enthalpy by locating the saddle point configuration. For this purpose, we generated a fcc crystallite containing some thousands of atoms (around 8000) and organized it into two regions. In the inner region (around 3500 atoms), which contains the defect, the atomic coordinates are free to relax (possibly subject to a given constraint, as in the present case), while the atoms in the outer region are held fixed at their perfect lattice sites. A brief description of the quasistatic approximation applied to $H_O\langle 100\rangle$ dumbbell migration is the following. We consider the case in which the defect jumps from site (000), where its orientation is [100], to site $(a/2,0,a/2)$ where its orientation is [001]. Configurations with different orientations along $\langle 100\rangle$ directions are equivalent. To locate the saddle point configuration we define a straight line connecting the coordinates of the migrating atom (one of the dumbbell atoms) in the two adjacent relaxed dumbbell configurations. Describing the coordinates of the migrating atom in the first configuration by the vector $R_i=(x_i,0,0)$ and in the second configuration by $R_f=(a/2,0,z_f)$, the path is given by $\Delta = R_f - R_i$. Starting from the first relaxed configuration, we take a small step along Δ, and then perform a constrained energy minimization in which only the $3N+2$ degrees of freedom perpendicular to Δ are allowed to relax. This procedure is then repeated successively, until the second configuration is reached. Note that the rigid boundary of the crystallite prevents the displacement of the whole lattice while the migrating atom is displaced along the path. Finally, the configuration corresponding to the maximum in the curve of energy vs displacement is associated with the saddle point, for which, in the present case, the forces on all of the atoms were found to be less than 10^{-6} eV/Å. Also, due to the high symmetry of the saddle point configuration, it is straightforward to reproduce it in a smaller cell subjected to constant (null) pressure and periodic boundary conditions, allowing an explicit verification of the saddle point character of the configuration in question. To this end, we computed the second-order force-constant matrix according to the procedure described in Ref. 19 and detected the presence of a unique unstable mode (negative eigenvalue). The unstable mode is along the migration path and the corresponding imaginary eigenfrequency, calculated for crystallites of different sizes up to 865 atoms, is seen to be well converged. It is worthwhile to note that the dumbbell migration takes place between nearest-neighbor sites by the combination of a translation and 90° rotation (reorientation).[1,5]

TABLE I. Calculated formation enthalpies of SIA's in Ni and Al at 0 K. *H* stands for dumbbell, *C* for crowdion, *O* for octahedral, and *T* for tetrahedral. Orientation of *H* and *C* is indicated. Values are in eV.

Defect configuration	$H_O\langle 100\rangle$	$H_C\langle 110\rangle$	$C\langle 110\rangle$	O	$H_T\langle 111\rangle$	T
Al	2.46	2.81	2.81	2.82	2.90	2.94
Ni	4.58	5.04	5.04	4.83	5.36	5.42

III. RESULTS

A. Interstitial formation properties

We have carried out MS structural optimizations for the six SIA configurations usually considered in the literature for the fcc structure.[5] The resulting formation enthalpy values are reported in Table I.

The results agree with experimental data (for example see Refs. 28 and 1), which indicate that in both metals the $H_O\langle 100\rangle$ structure is the most stable SIA configuration. For Al, the corresponding experimental value has been calculated according to $H_i^f = H_F^f - H_v^f$ where the right-hand side represents the difference between the Frenkel pair formation enthalpy and the vacancy formation enthalpy. The value obtained in this manner ranges between 3.0 (Ref. 29) and 3.6 eV.[30] The calculations of Lam *et al.*[31] based on long-range pair potentials give 2.89 eV for the $H_O\langle 100\rangle$ structure, while Gao *et al.*[32] obtain 2.71 eV with a modified version of the many-body potentials developed by Vitek *et al.*[33] which, although used for pure Al, are more appropriate for alloys. More recently, density functional theory calculations give 2.43 eV,[12] in excellent agreement with the present EA potential prediction (2.46 eV in Table I) and the one reported in Ref. 12 (2.47 eV). The small difference (less than 1%) between the two last values is attributed to the crystallite size. To the best of our knowledge, there are no reports of experimental values of H_i^f for Ni, but the present results are consistent with the calculations of Johnson,[34] who obtained a value of 4.08 eV using pair potentials, as well as with those of Gao *et al.*[32] and Foiles *et al.*[18] who obtained 4.85 and 5.05 eV, respectively, using EAM potentials.

In summary, most of the calculations in the literature agree that the $H_O\langle 100\rangle$ configuration is the SIA with the lowest formation energy, although the specific formation-

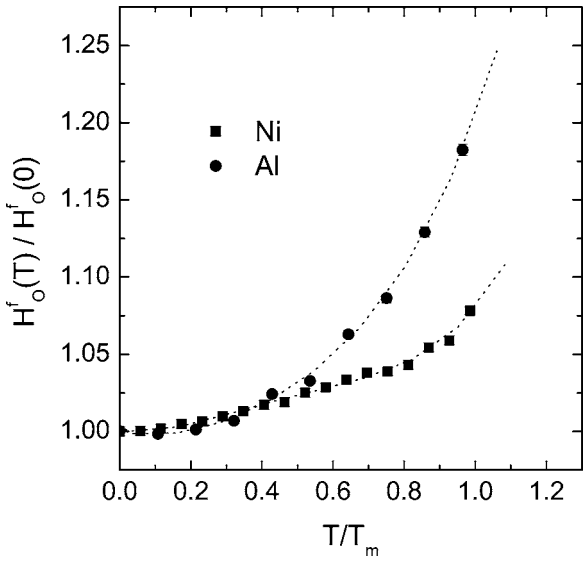

FIG. 1. H_O ⟨100⟩ formation enthalpy as a function of temperature. The enthalpy values are normalized to 0 K formation enthalpies, whereas the temperature axis has been scaled by the melting temperatures T_m=933 and 1726 K for Al and Ni, respectively. Dotted lines represent fourth-order polynomial regressions to the results.

enthalpy value is potential dependent. On the other hand, there is some disagreement with respect to the relative ranking of the other SIA configurations. For example, Table I shows essentially the same order of increasing SIA formation energy for both Ni and Al. For Al the ranking agrees with the findings of Foiles *et al.*,[18] for which the H_c configuration has the second-lowest formation energy. In contrast, the observations of Ackland *et al.*[35] suggest that this structure is not even metastable.

As a final consideration regarding the SIA's formation enthalpies, it is concluded that the calculations carried out in Al at zero temperature underestimate the experimental values. However, a reasonable agreement is obtained when considering temperatures close to the melting point. In this case, a formation enthalpy of 2.90 eV (see Fig. 1 below) is obtained from the calculations while the experimental value reported in Ref. 29 is 3.0 eV. Finally, it is noted that the formation energy calculated for the SIA is 3–4 times larger than the one for the vacancy, in agreement with the experimental evidence.[1,5]

The relaxation volumes for the H_O configuration have also been calculated, giving (in units of the atomic volume Ω) $\Delta V^{rel}_{\mathrm{Al}}=1.92$ and $\Delta V^{rel}_{\mathrm{Ni}}=2.34$. From the experimental side, measurements of Huang diffuse scattering of x rays on irradiated samples containing Frenkel pairs estimate 1.9 and 1.8,[36] respectively. Note that these results require an assumption about the vacancy-relaxation volume, for which the authors[36] have taken zero for Al and -0.22Ω for Ni, while the potentials used here predict -0.40Ω and -0.17Ω, respectively.[19]

The formation entropy calculated in the harmonic approximation according to Eq. (1) give $5.9k_B$ and $12.7k_B$ for the zero-temperature relaxed H_O configuration in Al and Ni, respectively. These are well-converged values obtained from crystallites of different size (865 atoms maximum). The present result for Al is approximately 10% higher than that previously quoted in Ref. 12 where the EA potential is also used. An even higher discrepancy, about 30%, is seen between the divacancy formation entropy values reported by the present authors and those of Refs. 12 and 13, namely, $3.45k_B$ (Ref. 19) and $2.50k_B$,[12] although for the vacancy the same value, $1.14k_B$,[12,14,19] is quoted.

Unfortunately, the information given in Ref. 12 is insufficient to clarify the mentioned differences. In particular, in Ref. 13 it is specified that the dynamical matrix is obtained by displacing the atoms in all three directions, this procedure giving $1.31k_B$ and $1.97k_B$ for the vacancy and divacancy formation entropy, respectively. As we will show later, HA results are significantly different from the ones obtained through the RW method.

The H_O formation enthalpies as a function of temperature obtained from MD simulations are shown in Fig. 1. The enthalpy and temperature axes have been scaled by, respectively, the 0 K formation enthalpy values (see Table I) and the melting temperatures (T_m=933 and 1726 K) for Al and Ni. The dotted lines represent fourth-order polynomial fits to the results. Comparing the results at the melting temperatures with those at 0 K, it is seen that the H_O formation enthalpies increase about 20% for Al, in very good agreement with Ref. 12, and 10% for Ni (curiously the corresponding percentages for the vacancy are the opposite, 10% for Al and 20% for Ni). Concerning the H_O relaxation volume, this increases up to 30%, which is seven times higher than the corresponding increase for the vacancy case.[12] These results are indicative of the role of anharmonic effects in the defect configuration properties. In addition, more than one interstitial configuration was found to play a role at high temperatures. In this situation, instead of the well-defined H_O formation enthalpy shown in Fig. 1, one would be measuring an effective formation enthalpy corresponding to the relative contributions of the different active configurations.

By using the analytical expressions for the enthalpies obtained from the fitting procedure, we integrate Eq. (2) to obtain the formation entropies as a function of temperature. As reference formation entropies (S_0), we use the values given by the HA for the 0 K relaxed defect structures. In this way, the formation free energy predicted by thermodynamic integration can be obtained (see TI HA in Fig. 2). In addition to the TI procedure we also compute the formation free energy directly by using the fully anharmonic RW switching method (also shown in Fig. 2 by the symbols). While in the case of Ni we find very good agreement between both computational techniques, there is a significant discrepancy for the case of Al. Following Ref. 14, this can be attributed to the chosen S_0 value. Effectively, in addition to the HA, S_0 can also be obtained from the slope of the formation free-energy curve calculated with the RW method at low temperatures. In this way, S_0 results as $(3.6\pm0.8)k_B$ for Al and $(13.1\pm0.5)k_B$ for Ni. Note the rather large discrepancy ($\approx$60%) between the S_0 predicted by both HA and RW methods for the case of Al. The origin of this discrepancy appears to be the same as that found in Ref. 14, and is related to the fact that the force constants involving the nearest-neighbor atoms of the defect show anomalous behavior for

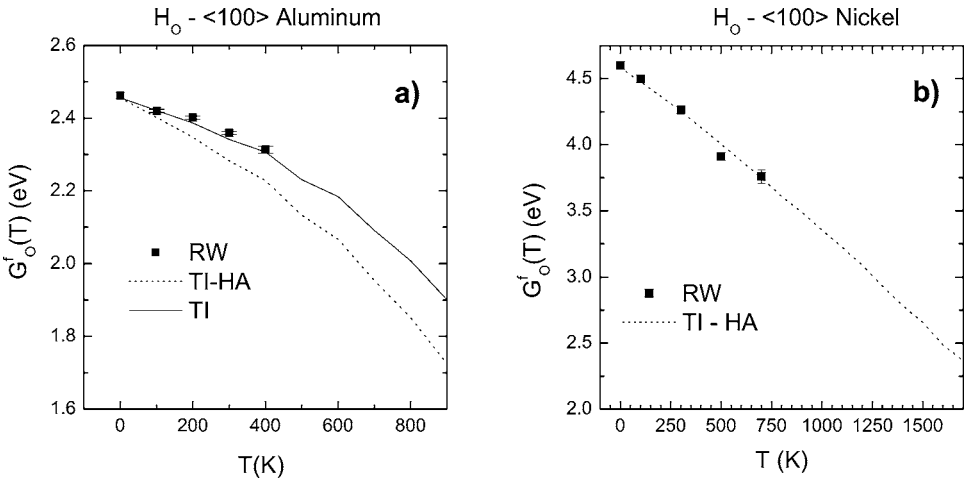

FIG. 2. H_O ⟨100⟩ formation free energies calculated by TI (lines) and RW (symbols) methods: (a) Al and (b) Ni. For the dotted lines, the reference formation entropy predicted by the HA is used. For the full line, the formation entropy predicted at low temperature by the RW method is used.

displacements below 0.02 Å, most likely due to an artifact of the Ercolessi-Adams potential. Such irregular behavior is absent for the Voter-Chen Ni potential. Finally, if instead of the HA value, the low-temperature RW estimate for the formation entropy is used in the TI procedure, the agreement between the resulting TI curve [shown as the full line in Fig. 2(a)] and the RW data becomes very good. Note that the SIA formation free energy shows a nonlinear temperature dependence for both materials, with more pronounced curvature for Al than for Ni. It is considered that, in addition to the anharmonic effects, several SIA configurations may be active at high temperatures, rendering the interpretation of the formation thermodynamics properties in terms of a unique and well-identified defect structure difficult.

B. Interstitial migration properties

The temperature dependence of the self-interstitial diffusion process is evaluated by MD. For this purpose we calculate the time evolution of the mean-square displacement to obtain D^* as a function of temperature according to Eq. (8). From the slopes of the corresponding Arrhenius plots (shown in Fig. 3), the effective migration energies can be evaluated. For Al, a straight plot with a migration energy value of 0.149 ± 0.004 eV is obtained for temperatures up to 900 K. However, for simulations at temperatures higher than melting, a slight upward curvature seems to appear in the overheated crystal, implying an increase in the effective migration energy. For Ni, the observed upward curvature allows one to consider two different temperature ranges. For the low one (400–900 K) a migration energy of 0.11 ± 0.01 eV is obtained, while for the high one (950–1700 K) the energy is seen to increase to 0.154 ± 0.003 eV. On the other hand, by applying the quasistatic approximation we obtain migration energy values of 0.16 eV (in agreement with Ref.12) and 0.13 eV for Al and Ni, respectively. Previous calculations, based on pair interatomic potentials, led to migration energies of 0.15 eV for both metals, showing consistency with the present results (see Refs. 31 for Al and 34 for Ni). In Al, experimental data available from electrical resistivity recovery measurements performed after low-temperature irradiation, as well as from elastic after-effect measurements, give 0.112 and 0.115 eV, respectively.[5] For Ni, electrical resistivity and magnetic after-effect measurements both estimate a migration barrier of 0.15 eV.[5]

In addition, we also carried out a detailed analysis of the interstitial jumps recorded from the MD runs to determine the jump frequencies and the involved jump mechanisms. Around 250 jumps were analyzed at each temperature for a reduced range, namely up to 700 and 900 K for Al and Ni, respectively.

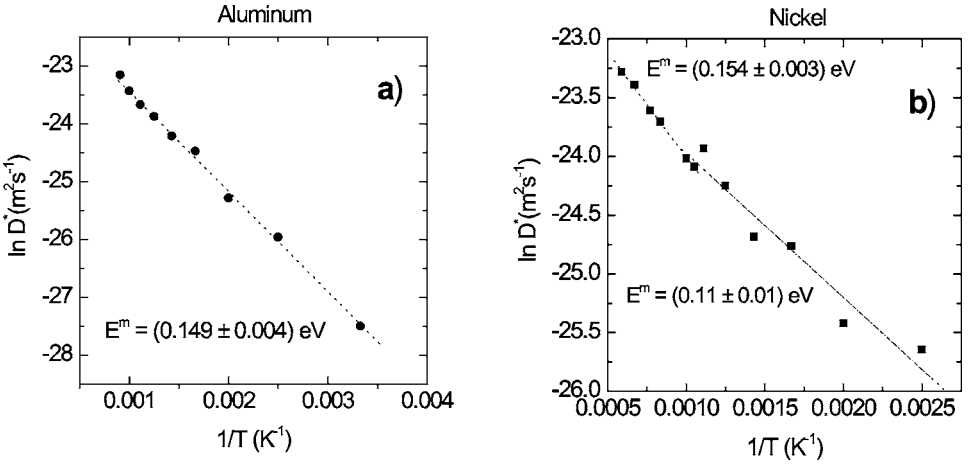

FIG. 3. Arrhenius plot of the atomic migration contribution (D^*) calculated for H_O by mean-square displacement: (a) Al and (b) Ni. Effective migration energies obtained through linear regressions (dotted lines) to the results are indicated. For Al the temperature range fitted is 300–900 K. For Ni two different temperature ranges are considered: 400–900 K and 950–1700 K.

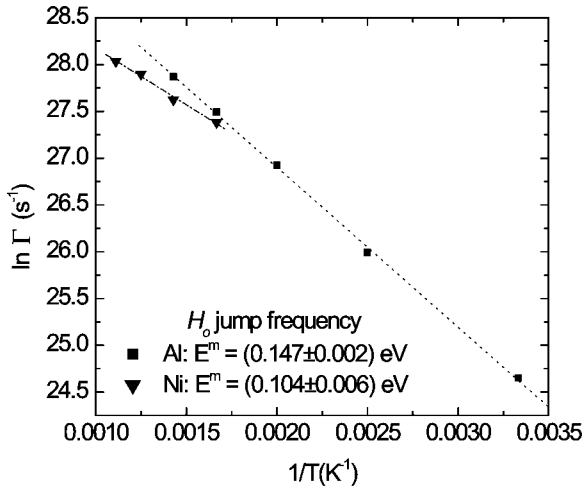

FIG. 4. Arrhenius plot of the H_O jump frequency. Temperature ranges 300–700 K (Al) and 600–900 K (Ni). The migration energies obtained through linear regressions (dotted lines) to the results are indicated.

For Al it was found that the H_O ⟨100⟩ configuration mainly migrates by the previously described single jumps. Only about 2.5% of the total jumps are double and triple, which are counted as two or three single jumps, respectively. Also, for about 2% of the cases, the dumbbell center of mass is seen to jump across distances that are larger than that for the single jumps via a different mechanism. After filtering out the oscillations that do not contribute to diffusion, the obtained jump frequency is plotted as a function of temperature in Fig. 4. The migration energy that results from this frequency plot is 0.147 ± 0.002 eV. The good agreement between the migration energy values obtained from mean-square displacement, molecular statics, and the frequency Arrhenius plot suggests that, in the explored temperature region (300–900 K), the migration process is controlled by one defect type only, namely, the H_O ⟨100⟩ dumbbell. Moreover, close inspection of the atomic coordinates for low temperatures and short simulation times reveals that the dumbbell remains oriented along directions of the ⟨100⟩ type most of the time. Accordingly, the TI calculations performed to evaluate the ⟨100⟩ dumbbell formation free energies in Fig. 2 are expected to be reliable.

For Ni, the jump frequency Arrhenius plot depicted in Fig. 4 for a reduced low-temperature range corresponds to a defect migration energy of 0.104 ± 0.006 eV, in close agreement with mean-square displacement and molecular static calculations. In this case, other interstitial configurations in addition to H_O are found to contribute to the dynamics as the temperature increases. By inspection of the atomic coordinates it is observed that, although the defect spends most of the time in the H_O ⟨100⟩ dumbbell configuration, it also samples other intermediate configurations that, for example, have the H_C ⟨110⟩ (or equivalent) character for relevant periods of time. The relative importance of these intermediate configurations increases with temperature, being around 10% at 600 K and 35% at 900 K. The complexity associated with these intermediate configurations precluded us from evaluating well-defined jump frequencies at higher temperatures. Correspondingly, the interstitial migration enthalpy obtained from mean-square displacement calculations, slightly higher than that for the low-temperature range, represents an effective value that averages the contributions of the various intermediate configurations. In a similar fashion, the TI calculations for high temperatures presented in the section above should be expected to represent an effective formation free energy, involving an average over several distinct interstitial configurations.

IV. DISCUSSION AND CONCLUSIONS

The enthalpy, volume, entropy, and Gibbs free energy values associated with the formation of the H_O ⟨100⟩ dumbbell in Al and Ni have been computed as a function of temperature using different atomistic techniques. A comparison with previous calculations and experimental results is also presented.

The formation free energy has been calculated using both thermodynamic integration and reversible work methods. The first requires a reference entropy value S_0 that is usually calculated within the harmonic approximation. In the case of Ni the formation free energies obtained with TI are in excellent agreement with those predicted by the RW method. For Al, however, a significant discrepancy is observed similarly to that previously found for the vacancy case when the same interatomic potential is used.[14] Its origin may lie in the fact that the force constants connecting the nearest-neighbor atoms of the defect show anomalous behavior for displacements below 0.02 Å, while for Ni, the corresponding behavior is more regular. As a consequence, the harmonic low-temperature formation entropy S_0 might not be reliable for the Ercolessi-Adams potential. Specifically, the fully anharmonic result obtained with the RW method is $(3.6 \pm 0.8)k_B$ whereas the HA value is estimated to be $5.9k_B$. For Ni there is no such discrepancy, and both techniques are in close agreement for the low-temperature formation entropy [$12.7k_B$ for the HA and $(13.1 \pm 0.5)k_B$ for the RW method].

At the melting point, the interstitial formation entropies are seen to increase by factors of approximately 3.5 and 1.5, being $12.9k_B$ and $17.6k_B$, respectively, for Al and Ni. The present result for Al is approximately 40% higher than that of Ref. 12. The increase of the entropy reveals the role of the anharmonic effects and is consistent with the predictions of the interstitialcy theory, according to which values in the range $(10-20)k_B$ should be expected[2–4,7,16] for the self-interstitials.

A comparison between the present calculations and those reported in Ref. 14 suggests that the vacancy concentration in Al near melting is 3.2×10^{-4}, whereas that of the interstitial is around 7×10^{-11}. The corresponding values for Ni are 3×10^{-4} and 2.9×10^{-7}, respectively. These results imply that, although larger than usually assumed, the interstitial concentration near melting is still relatively low compared to the thermal-equilibrium vacancy concentration. In addition, the corresponding equilibrium concentration of divacancies calculated according to the results from Ref. 14, 1.6×10^{-6} for Al and 2.5×10^{-6} for Ni, are also higher than those for

self-interstitials. These findings, particularly for Al, are in disagreement with the theoretical results reported for copper in Ref. 16, according to which the self-interstitial concentration is similar to that of divacancies at the melting temperature.

From the experimental side, the C_{44} shear modulus measured in Al by Granato[7] gives $(1.7\pm0.6)\times10^{-4}$ as the best estimate for the interstitial concentration just below the melting temperature. To obtain this result, a formation enthalpy of 2.5 ± 0.5 eV was assumed, giving a formation entropy estimate of $22k_B$. While our estimate for the formation enthalpy at the melting point (2.90 eV) is in reasonable agreement with the previous value, our estimate for the formation entropy ($12.9k_B$) remains significantly lower. Although the quality of the potential is certainly at issue, the limitations of the experimental technique also need to be taken into consideration. As Granato points out,[7] although the technique is useful to detect a sharp high-temperature shear modulus increase (attributed to interstitials), it did not provide data with sufficient resolution to determine the interstitial formation enthalpy and entropy separately.

Regarding the energetics of self-interstitial migration, good agreement is found between experimental data[5] and the present calculations. In Al, the linearity of the Arrhenius plots in the studied temperature range (up to 700 and 900 K for jump frequency and mean-square displacement determinations, respectively) suggests that the self-interstitial remains in a single configuration, the H_O $\langle100\rangle$ dumbbell, and migrates according to its typical mechanism. For higher temperatures, however, the deviation from the linear plot can be attributed to the contribution of other mechanisms. For Ni, a slight upward curvature is observed in the Arrhenius plot obtained from mean-square displacement determinations for temperatures up to 1700 K. This behavior suggests that the H_O $\langle100\rangle$ is not the only active configuration. Effectively, increasing contributions of different jump mechanisms and/or interstitial configurations have been observed as the temperature increases.

Finally, the contributions of divacancies and self-interstitials to the tracer self-diffusion coefficient D^T at high temperatures can be compared. For a single defect type this can be calculated through the relation $D^T=1/6d^2fC\Gamma$, where d is the jump distance, f the correlation factor, and C and Γ the defect equilibrium concentration and jump frequency, respectively. In molecular dynamics simulations free of constraints, it is observed that the divacancy dissociates as the temperature increases.[19] This behavior precludes the direct evaluation of Γ at high temperatures. Nevertheless, approximated values can be estimated from low-temperature results. In Ni, the migration properties calculated[19] for temperatures up to 1000 K are then extrapolated to temperatures near melting. In Al, due to the divacancy instability observed at relatively low temperatures, the migration results obtained from molecular static simulations, combined with the RW prediction for the divacancy concentration, are employed.[19] At 900 K, the following values (in m^2/s) are then obtained for the contributions of different defects to D^T in Al: 3.1×10^{-13} (vacancies), 5.2×10^{-14} (divacancies), 9.2×10^{-19} (interstitials). In Ni at 1700 K, the corresponding values (in m^2/s) are 1.7×10^{-12} (vacancies), 1.3×10^{-14} (divacancies), and 5.7×10^{-15} (interstitials). The values show the small contribution of self-interstitials to self-diffusion in Al, in contrast to the case of Ni, where the role of self-interstitials should not be disregarded. This conclusion, consistent with previous studies,[16] is mainly related to the fact that the Ni self-interstitial formation entropy is significantly larger than that of the divacancy, the difference being independent of anharmonic effects.

ACKNOWLEDGMENTS

This work was supported by CNEA-Argentina Grant No. (P5-PID-35-2-01) and SECyT-Argentina Grant No. (PICT 12 -06164-99) and Universidad Nacional del Comahue (Project No. I103). M.K. gratefully acknowledges financial support from the Brazilian agencies FAPESP and CNPq. Part of the calculations were performed at CENAPAD/SP.

[1] P. Ehrhart, in *Atomic Point Defects in Metals: Crystal and Solid State Physics*, edited by H. Ullmaier, Landolt-Börnstein, New Series, Group III, Vol. 25 (Springer-Verlag, 1991), p. 202.
[2] A. V. Granato, Phys. Rev. Lett. **68**, 974 (1992).
[3] C. A. Gordon, A. V. Granato, and R. O. Simmons, J. Non-Cryst. Solids **205-207**, 216 (1996).
[4] C. A. Gordon and A. V. Granato, Mater. Sci. Eng., A **370**, 83 (2004).
[5] H. J. Wollenberger, in *Physical Metallurgy*, edited by R. W. Cahn and P. Haasen (Elsevier Science, Amsterdam, 1996), Vol. 2, p. 1622.
[6] P. H. Dederichs, C. Lehmann, H. R. Schober, A. Scholz, and R. Zeller, J. Nucl. Mater. **69-70**, 176 (1978).
[7] A. V. Granato, J. Phys. IV **6**, C8-1 (1996).
[8] A. Seeger and H. Mehrer, in *Vacancies and Interstitials in Metals*, edited by A. Seeger, D. Shumacher, W. Schilling, and J. Diehl (North-Holland, Amsterdam, 1970), p. 1.
[9] H. M. Gilder and D. Lazarus, Phys. Rev. B **11**, 4916 (1975).
[10] N. Sandberg and G. Grimvall, Phys. Rev. B **63**, 184109 (2001).
[11] K. Carling, G. Wahnström, T. R. Mattsson, A. E. Mattsson, N. Sandberg, and G. Grimvall, Phys. Rev. Lett. **85**, 3862 (2000).
[12] N. Sandberg, B. Magyari-Kope, and T. R. Mattsson, Phys. Rev. Lett. **89**, 065901 (2002).
[13] K. M. Carling, G. Wahnström, T. R. Mattsson, N. Sandberg, and G. Grimvall, Phys. Rev. B **67**, 054101 (2003).
[14] M. de Koning, S. Ramos de Debiaggi, and A. M. Monti, Defect Diffus. Forum **224-225**, 59 (2003).
[15] M. de Koning, S. Ramos de Debiaggi, and A. M. Monti, Phys. Rev. B **70**, 054105 (2004).
[16] K. Nordlund and R. S. Averback, Defect Diffus. Forum **188-190**, 59 (2001).
[17] M. J. Sabochick and N. Q. Lam, Phys. Rev. B **43**, 5243 (1991).

[18] S. M. Foiles, M. I. Baskes, and M. S. Daw, Phys. Rev. B **33**, 7983 (1986).
[19] M. García Ortega, S. B. Ramos de Debiaggi, and A. M. Monti, Phys. Status Solidi B **234**, 506 (2002).
[20] F. Ercolessi and J. B. Adams, Europhys. Lett. **26**, 583 (1994).
[21] A. F. Voter and S. P. Chen, in *Characterization of Defects in Materials*, edited by R. W. Siegel, J. R. Weertman, and R. Sinclair, MRS Symposia Proceedings No. 82 (Materials Research Society, Pittsburgh, 1987), p. 175.
[22] M. W. Finnis and J. E. Sinclair, Philos. Mag. A **50**, 45 (1984).
[23] R. D. Hatcher, R. Zeller, and P. H. Dederichs, Phys. Rev. B **19**, 5083 (1979).
[24] D. Frenkel and B. Smit, in *Understanding Molecular Simulation* (Academic Press, San Diego, 1996), p. 152.
[25] H. J. C. Berendsen and W. F. van Gunsteren, in *Molecular Dynamics Simulations of Statistical Mechanical Systems, Proceedings of the International School of Physics "Enrico Fermi," Course 97*, edited by G. Ciccoti and W. G. Hoover (North-Holland, Amsterdam, 1986), p. 43.
[26] S. M. Foiles, Phys. Rev. B **49**, 14930 (1994).
[27] M. de Koning, A. Antonelli, and S. Yip, Phys. Rev. Lett. **83**, 3973 (1999).
[28] P. Ehrhart, J. Nucl. Mater. **69-70**, 200 (1978).
[29] H. Wollenberger and J. Wurm, Phys. Status Solidi **9**, 601 (1965).
[30] W. Schilling and P. Tischer, Z. Angew. Phys. **22**, 56 (1967).
[31] N. Q. Lam, N. V. Doan, and Y. Adda, J. Phys. F: Met. Phys. **10**, 2359 (1980).
[32] F. Gao, D. J. Bacon, and G. J. Ackland, Philos. Mag. A **67**, 275 (1993).
[33] V. Vitek, G. J. Ackland, and J. Cserti, in *Alloy Phase Stability and Design*, edited by G. M. Stocks, D. P. Pope, and A. F. Giamei, MRS Symposium Proceedings No. 186 (Materials Research Society, Pittsburgh, 1990), p. 227.
[34] R. A. Johnson, Phys. Rev. **145**, 423 (1966).
[35] G. J. Ackland, G. Tichy, G. Vitek, and M. W. Finnis, Philos. Mag. A **56**, 735 (1987).
[36] O. Bender and P. Ehrhart, J. Phys. F: Met. Phys. **13**, 911 (1983).